Geoscientific
Model Development

Evaluation of high-resolution GRAMM–GRAL (v15.12/v14.8) NO$_x$ simulations over the city of Zürich, Switzerland

Antoine Berchet[1], Katrin Zink[1], Dietmar Oettl[2], Jürg Brunner[3], Lukas Emmenegger[1], and Dominik Brunner[1]

[1]Empa, Swiss Federal Laboratories for Materials Science and Technology, Dübendorf, Switzerland
[2]Air Quality Control, Government of Styria, Landhausgasse 7, 8010 Graz, Styria, Austria
[3]Office for Environment and Health protection, City of Zürich, Zürich, Switzerland

Correspondence to: A. Berchet (antoine.berchet@empa.ch)

Abstract. Hourly NO$_x$ concentrations were simulated for the city of Zürich, Switzerland, at 10 m resolution for the years 2013–2014. The simulations were generated with the nested mesoscale meteorology and micro-scale dispersion model system GRAMM–GRAL (versions v15.12 and v14.8) by applying a catalogue-based approach. This approach was specifically designed to enable long-term city-wide building-resolving simulations with affordable computation costs. It relies on a discrete set of possible weather situations and corresponding steady-state flow and dispersion patterns that are pre-computed and then matched hourly with actual meteorological observations. The modelling system was comprehensively evaluated using eight sites continuously monitoring NO$_x$ concentrations and 65 passive samplers measuring NO$_2$ concentrations on a 2-weekly basis all over the city. The system was demonstrated to fulfil the European Commission standards for air pollution modelling at nearly all sites. The average spatial distribution was very well represented, despite a general tendency to overestimate the observed concentrations, possibly due to a crude representation of traffic-induced turbulence and to underestimated dispersion in the vicinity of buildings. The temporal variability of concentrations explained by varying emissions and weather situations was accurately reproduced on different timescales. The seasonal cycle of concentrations, mostly driven by stronger vertical dispersion in summer than in winter, was very well captured in the 2-year simulation period. Short-term events, such as episodes of particularly high and low concentrations, were detected in most cases by the system, although some unrealistic pollution peaks were occasionally generated, pointing at some limitations of the steady-state approximation.

The different patterns of the diurnal cycle of concentrations observed in the city were generally well captured as well. The evaluation confirmed the adequacy of the catalogue-based approach in the context of city-scale air pollution modelling. The ability to reproduce not only the spatial gradients but also the hourly temporal variability over multiple years makes the model system particularly suitable for investigating individualized air pollution exposure in the city.

1 Introduction

The urban population has grown steadily in the past century and already reached 50 % globally and more than 75 % in many developed countries. Urban areas with high population density are hotspots of air pollutant emissions, raising concerns regarding increased mortality and morbidity (Cohen et al., 2004; Jerrett et al., 2004; Beelen et al., 2013). Some of the most critical air pollutants in terms of health effects are particulate matter (PM) and NO$_2$, whose levels exceed national and WHO standards in many urban areas (e.g. in Europe; Beelen et al., 2014). In Switzerland, and more particularly in urban centres such as the Zürich area, despite improving trends, the urban population is still exposed to harmful levels of PM smaller than 10 μm (PM$_{10}$) and NO$_2$ (Heldstab et al., 2011). Health effects of air pollution are well documented through numerous epidemiological studies (Brunekreef and Holgate, 2002; Beelen et al., 2008; Raaschou-Nielsen et al., 2013), but these studies rely on coarse estimates of the average population exposure as it is very challenging to account for the steep gradients and

large temporal variability of air pollutant concentrations in cities (Jerrett et al., 2004; Beelen et al., 2008, 2013). Computing individualized pollution exposure in urban areas requires high-resolution simulations, with at least hourly resolution and spanning long periods of time (years to decades) since health impacts can be triggered by both short-term exceedances of pollution thresholds or long-term continuous exposure to high pollution levels (Van Roosbroeck et al., 2006; Beelen et al., 2008; Lelieveld et al., 2013). Individualized exposure is not only useful for epidemiological studies, but also for air quality plans designed by cities to reduce the direct and indirect social and economic costs of air pollution (e.g. Lelieveld et al., 2013). Current air quality plans are generally lacking a systematic cost–benefit assessment of different mitigation measures due to the lack of affordable model solutions that satisfy the demanding requirements in terms of resolution, temporal coverage and source-specific information (Miranda et al., 2015).

In the present study, we focus on NO_x, an air pollutant with particularly large spatial and temporal gradients due to its short lifetime (e.g. Vardoulakis et al., 2002). Representing the gradients in NO_x concentrations in cities is not yet achievable by standard chemistry-transport models, as they are limited to horizontal resolutions of typically a few kilometres (e.g. Terrenoire et al., 2015). Recent progress in computational fluid dynamics (CFD) models makes it possible to run high-resolution dispersion simulations on the city scale (Li et al., 2006; Kumar et al., 2009, 2011; Di Sabatino et al., 2013). However, the prohibitive computational cost of these simulations prevents their application in the context of long-term urban exposure assessment (Parra et al., 2010). Currently, the most widely used models for urban exposure assessment and regulatory applications are models with a simplified parametrization of pollutant dispersion (e.g. Gaussian plume) such as ADMS (Stocker et al., 2012), AERMOD (Rood, 2014), SIRANE (Soulhac et al., 2011), IFDM (Lefebvre et al., 2011) or OSPM (Kakosimos et al., 2010). When correctly parametrized and calibrated, these models offer a reliable representation of the average concentration distribution in cities (Soulhac et al., 2011; Briant et al., 2013; Brandt et al., 2013). However, they have difficulties in representing the dispersion in complex building and street canyon configurations and properly reproducing the temporal (hourly) variability due to varying meteorology (e.g. Soulhac et al., 2012; Ottosen et al., 2015). With the growing availability of urban air pollution observations due to recent advances in (low-cost) sensor technology (Jiao et al., 2016; Gao et al., 2016), land-use regression (LUR) models are increasingly being used for air pollution assessment (Kumar et al., 2015b; Heimann et al., 2015), offering a performance comparable to CFD full physics models (Beelen et al., 2010). Yet LUR models need a large amount of in situ observations at strategic locations to represent the full spatial and temporal variability (Duvall et al., 2016; Mueller et al., 2015, 2016; Hasenfratz et al., 2015) and cannot be ex-tended backward in time to satisfy the needs of long-term epidemiological studies.

Considering the respective strengths and limitations of the standard urban air pollution modelling systems, Berchet et al. (2017b) proposed a novel method that involves taking advantage of high-resolution accurate CFD modelling while keeping computational costs affordable, by using a catalogue-based approach merged with routinely available meteorological observations. They showed that it was computationally feasible to simulate hourly concentration maps over multiple years at building-resolving resolution, which successfully capture most of the variability in NO_x concentrations caused by variations in air flow and atmospheric stability. The main purpose of the present study is to provide a comprehensive evaluation of the above-mentioned method for NO_x concentrations in Zürich, Switzerland, for the years 2013–2014. The modelling domain covers the entire urban area of Zürich and includes 8 continuous NO_x monitoring sites as well as 65 NO_2 passive samplers. We demonstrate the high quality and robustness of the catalogue-based modelling system for hourly and daily concentrations. Furthermore, we identify sources of errors and uncertainties in the modelling system and propose additional steps to improve the methodology.

In Sect. 2, the modelling chain applied to generate time series of pollution maps is described. In Sect. 3, the set-up for the city of Zürich is presented including the available in situ observations, the emission inventory and auxiliary data sets. In Sect. 4, the performance of the model in terms of spatial distribution and temporal variability is evaluated with in situ NO_x and NO_2 measurements.

2 Approach and modelling system

2.1 Catalogue-based approach

Our approach relies on explicit physical simulations of air flow and pollutant dispersion. Such simulations on a city-wide domain must account for the cascade of scales influencing flow patterns, from the synoptic to the street and building scale. The synoptic scale defines the general meteorological conditions and the mean direction and strength of the large-scale flow in the city region. Land-use and topography restructure the synoptic weather on the regional scale by generating mesoscale phenomena such as thermally driven land–lake breezes as well as up- and down-slope circulations, urban heat islands, and channelling and blocking of the flow by the topography. Inside the city, these regional conditions are further modified on the micro-scale by buildings and other obstacles such as vegetation. To properly account for this cascade of scales, our model approach is based on a three-step procedure using the models GRAMM v15.12 (Graz mesoscale model; Almbauer et al., 2000) and GRAL v14.8 (Graz Lagrangian model; Oettl, 2015b), further described in Sect. 2.2: (i) mesoscale air flow accounting for topography
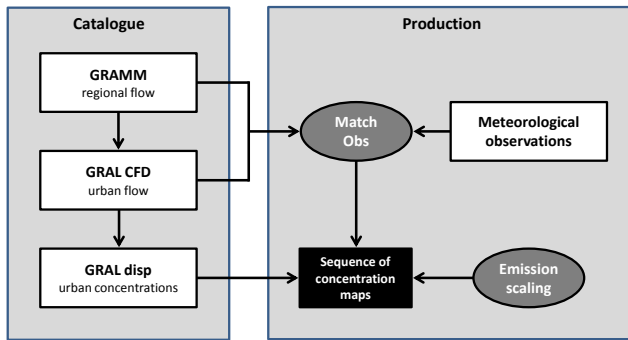
Figure 1. Scheme of the multi-step procedure to generate a sequence of hourly steady-state concentration maps from a catalogue of pre-computed wind and concentration fields. The dark grey ovals are the method steps for generating time series of concentrations from the catalogue. Light grey rectangles denote intermediary products and inputs in the system.

and land-use effects is computed by GRAMM for a larger domain centred on the city; (ii) micro-scale air flow inside the city, accounting for the effects of buildings on flow and turbulence patterns, is inferred with the GRAL model, forced by GRAMM outputs; and (iii) Lagrangian dispersion computations are carried out by the dispersion module of GRAL, constrained by the micro-scale wind fields generated by GRAL. The GRAMM–GRAL system is briefly described in Sect. 2.2.

Simulating the full transient evolution of the atmosphere over a multi-year period is not yet feasible at building-resolving resolution (i.e. better than 10 m) for a whole city with current computing resources (e.g. Parra et al., 2010). Therefore, we approximate the full temporal dynamics by a sequence of steady-state solutions selected from a pre-computed catalogue as described in Berchet et al. (2017b). This catalogue is a discrete representation of all possible weather situations in terms of atmospheric stability and of large-scale wind speed and direction at the boundaries of the domain. Binning large-scale wind directions and speeds into 36 (10° each) and 7 (from 0.25 to 7 m s^{-1}) categories, respectively, with seven possible Pasquill–Gifford classes for atmospheric stability as defined by the US Environment Protection Agency (2000), leads to a catalogue of 1008 physically meaningful reference weather situations. As illustrated in Fig. 1, this catalogue is computed in a three-step procedure which subsequently generates the mesoscale winds computed with GRAMM and the corresponding urban-scale winds and air pollutant concentrations computed with GRAL. The complete procedure was implemented as a Python library in Berchet et al. (2017a).

Once the catalogue is available, a sequence of hourly weather situations is built based on in situ observations of wind speeds and directions in and around the city. For every hour of the simulated period, the weather situation in the catalogue is selected whose associated wind field best matches the in situ observations. As demonstrated in Berchet et al. (2017b), vertical stability and mesoscale flow patterns are intimately linked such that the stability can be sufficiently constrained by matching only the winds at a few selected locations in the model domain. The time series of hourly concentration distributions is then deduced directly from the sequence of weather situations. Generating concentration fields directly from matched weather situations and steady-state dispersion simulations implicitly attributes the influence of emissions at a specific time stamp entirely to the same hour, even though some virtual particles remain longer than 1 h in the domain. It thus prevents accounting for the accumulation of air pollutants over subsequent hours and for flow changes during such periods of accumulation, but performs well in most cases as demonstrated in Sect. 4. Transport from remote sources outside of the simulation domain is represented by background concentrations measured at a rural site near the city and added to the simulated concentrations. This approach implicitly assumes that background concentrations are uniform over the whole modelling domain, even though small horizontal and vertical gradients may exist, especially in our set-up with complex topography. A future refinement of the approach would thus be desirable. To account for emissions varying independently from the weather, concentration maps in the catalogue are first computed using yearly average emissions and then scaled for each hour according to varying emission activity (e.g. diurnal cycle of traffic emissions). Since not all types of emissions follow the same temporal profile, emissions are divided into categories (see Sect. 3.3 and Table 1), for each of which a catalogue of concentration distributions is computed, and then scaled independently.

Thus, our catalogue-based method can be summarized by the following equation. At a given hour h and point $\boldsymbol{x}$, the simulated concentration can be written as follows:

$$c(\boldsymbol{x}, h) = c_{\text{background}}(h) + \sum_{i \in \text{sectors}} \tau_i(h) \times c_i(\eta(h), \boldsymbol{x}), \qquad (1)$$

where τ_i is the unitless temporal profile of emissions for each sector i, $c_{\text{background}}(h)$ the background concentrations measured at the distant site, and $c_i(\eta(h), \boldsymbol{x})$ the simulated concentration field for sector i and weather situation $\eta(h)$, obtained with yearly average emissions. The weather situation $\eta(h)$ best matching the meteorological observations at hour h is selected following Eq. (3) of Berchet et al. (2017b).

Our modelling approach requires routinely available wind observations in the vicinity of the city of interest and a background pollution observation site in the rural environment of the city. Berchet et al. (2017b) concluded that 5–6 wind observation sites distributed around the city are generally sufficient to represent the variability of weather situations. The emission variability in Eq. (1) is determined from a wealth of information and models, including traffic counts (see Sect. 3) as proxies of emission variability. With such a catalogue-based approach, multi-year hourly physical simulations can be carried out at a cost of only 1–2 months of hourly simula-

tions. The drawback of the approach is that the full transient dynamics are replaced by a sequence of steady-state solutions, but as will be shown in this evaluation, this has only limited impact on the results.

2.2 GRAMM–GRAL modelling system

The catalogue-based approach relies on meteorological and on micro-scale flow and air pollutant dispersion simulations. The mesoscale simulations are carried out by GRAMM (Oettl, 2015a, 2016) and the micro-scale simulations by GRAL v14.8 (Oettl, 2015b). GRAMM is a non-hydrostatic model solving the conservation equations for mass, enthalpy, momentum and humidity. It accounts for contrasts in land use and corresponding surface fluxes of heat, momentum and humidity, and it has been specifically designed for operation in steep topography. The large-scale weather conditions (wind speed and direction, stability class) of the catalogue are translated into parametrized vertical profiles of winds, temperature and pressure, as well as Obukhov length for different stability classes (following the Pasquill–Gifford classification: in the following, from A, very unstable situation, to G, extremely stable) to constrain the initial and boundary conditions of GRAMM simulations, as further detailed in Berchet et al. (2017b), Oettl (2015a) and Oettl (2016).

GRAL is nested into GRAMM and is run here in diagnostic mode at 10 m resolution, which is different from Berchet et al. (2017b) where GRAL was run in prognostic mode at 5 m resolution. In diagnostic mode, the flow field around buildings is computed by interpolating GRAMM wind fields on a fine Cartesian grid, and assuming a logarithmic wind profile close to walls. Finally, mass conservation is achieved by applying a Poisson equation to establish a pressure field to correct the velocities. In the prognostic mode, the flow is explicitly computed by forward integration of a set of prognostic equations. We chose here to use the diagnostic mode as the computation costs are lower, which allowed us to simulate a much larger domain covering the complete urban area of Zürich (see Sect. 3.1). We found only minor differences between the simulations with the two modes and resolutions and thus discuss only the results for the diagnostic mode in the following. Lagrangian dispersion simulations are computed with virtual particles released from prescribed emission sources (Oettl and Hausberger, 2006; Oettl, 2014) and transported according to the pre-computed GRAL wind fields. Turbulent diffusion is represented by specific Langevin equations applicable for the full range of wind speeds, in particular for low wind speeds (Anfossi et al., 2006).

2.3 Evaluation approach

The European Commission expert panel FAIRMODE (Forum for Air quality Modelling in Europe) has been tasked with defining quality objectives and performance criteria for air quality models, following the Directive 2008/50/EC of the European Parliament (EC, 2001). These criteria have been described in Thunis et al. (2012) and Pernigotti et al. (2013). They are base on the following metrics:

- normalized mean bias NMB $= \frac{\overline{S} - \overline{O}}{\overline{O}}$, with $\overline{S}$ and $\overline{O}$ the average simulations and observations, respectively;

- mean fractional bias NFB $= \sum 2 \frac{s_i - o_i}{s_i + o_i}$, with s_i and o_i individual simulated and observed values, respectively;

- relative percentile error RPE, i.e. the relative error of the 90th percentile;

- FAC2, the fraction of simulations falling into a factor 2 of the observations;

- MQO, the model quality objective, $\frac{RMSE}{2U}$, with RMSE denoting the root mean square error and U the average model–observation uncertainty.

The performance criteria specify thresholds for the above-mentioned metrics. They are either defined as an absolute value (50 % for RPE and FAC2; 1 for MQO) or are dependent on the model–observation uncertainty. In a pragmatic approach, the uncertainty U was chosen proportional to the observed and simulated values in Thunis et al. (2012). To adapt these definitions to urban simulations in the presence of very high concentration gradients, we add the range of simulated values within a 15 m radius around a given observation site to the uncertainties. Therefore, traffic sites with very high local gradients have higher uncertainties than urban background sites. Scores are presented for two different simulated time series representing the concentrations at the exact location of the observation sites (reference), and the minimum of all concentrations in a radius of 15 m horizontally and 2 m vertically (minimum), respectively. The motivation for this will be presented in Sect. 4.1.

3 Setup for the city of Zürich

3.1 Model domain

The model domain centred on the city of Zürich, Switzerland, is illustrated in Fig. 2. The region is characterized by mountain ridges channelling the air flow and separating valleys where the population lives and where air pollution accumulates. In addition, the city of Zürich is located at the northern extremity of Lake Zürich, an elongated lake that covers an area of 120 km^2, large enough to generate weak land–lake breeze circulations. Mesoscale simulations with GRAMM are carried out in a domain spanning a region of 30×30 km^2, with a horizontal resolution of 100 m. The simulation domain was chosen to be large enough to allow all topographic features potentially affecting the flow in the city to be represented. The domain extends vertically from the surface to 3000 m above ground with 22 geometrically spaced
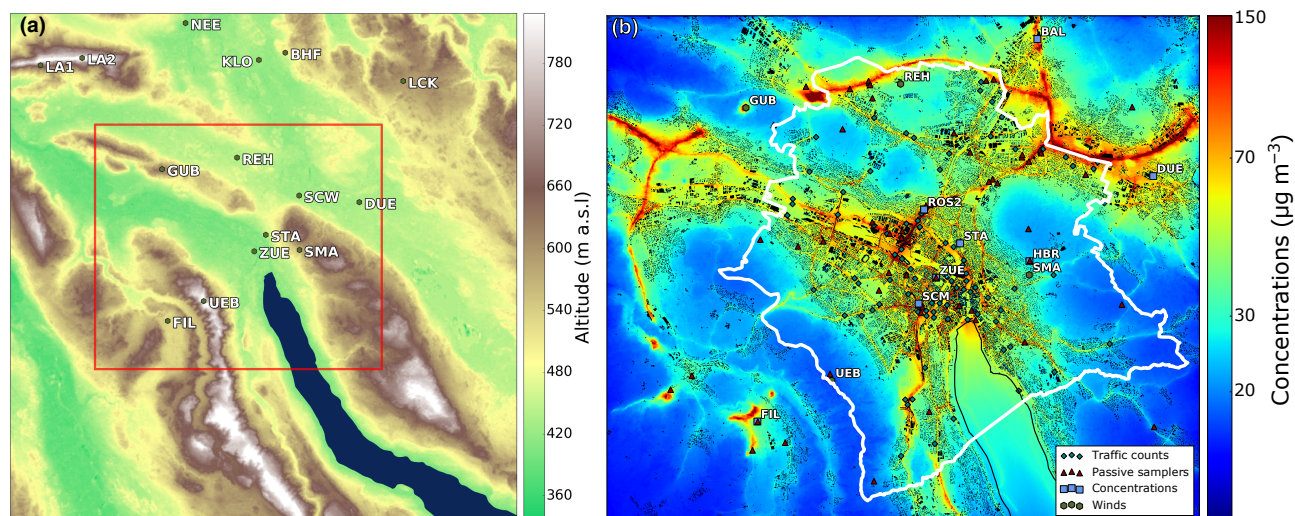
Figure 2. Simulation domains for the models GRAMM and GRAL. **(a)** GRAMM domain and wind measurement sites used in the match-to-observations procedure. The red rectangle is the domain covered by GRAL. **(b)** GRAL domain with in situ observation sites overlaid on the 2013–2014 average NO$_x$ concentrations as simulated by the modelling system. The political borders of the city are delimited by the white line.

layers varying in thickness between 12 m close to the surface and 500 m in the free troposphere.

Dispersion simulations are computed on a smaller domain encompassing the whole city of Zürich and most of its outskirts, including some suburban agglomerations and industrial areas. GRAL is run at 10 m horizontal and 2 m vertical resolution on this $17 \times 14\,\text{km}^2$ domain. Due to the hilly topography, highways are built through numerous tunnels, creating NO$_x$ emission hotspots at ventilation shafts and tunnel portals, which can optionally be treated in GRAL with a specific algorithm, described in Oettl et al. (2002), or simply as point sources at the tunnel gates.

3.2 General model inputs

As mentioned in Sect. 2, air flow computations require information on the topography, land-use types and buildings. Topographical information was taken from the ASTER GDEM2 (Advanced Spaceborne Thermal Emission and Reflection Radiometer – Global Digital Elevation Map Version 2) data set at a resolution of 30 m and projected to the 100 m GRAMM grid and linearly interpolated to the 10 m GRAL grid. Information on land use (water bodies, forests, etc.) at a resolution of 100 m was taken from the CORINE Land Cover data set (version CLC2006) distributed by the European Environment Agency. The 44 CORINE land-use classes are translated into typical values for roughness length, heat capacity, thermal conductivity, albedo and soil moisture for GRAMM computations. GRAL uses land-use classes in terms of roughness length to account for surface drag caused by different types of vegetation, whereas the drag imposed by buildings is represented explicitly. The CORINE data set

is projected similarly to ASTER to the GRAMM and GRAL grids. Three-dimensional building information inside the city of Zürich was deduced from a vectorial building inventory provided by the municipality of Zürich. Buildings outside of the city are taken from the nationwide vectorial data base swissBUILDINGS3D v2.0, provided by the Swiss Federal Office of Topography, Swisstopo. Vectorial building shapes were projected to the 10 m GRAL grid, i.e. buildings are represented by individual blocks of 10 m × 10 m horizontal size.

3.3 Emission data

Emission data are deduced from two very detailed inventories produced by the municipal (Umwelt- und Gesundheitsschutz, UGZ) and cantonal (Amt für Abfall, Wasser, Energie und Luft, AWEL) environment authorities. Inventory information is detailed in Table 1. Both inventories are spatially explicit bottom-up inventories based on activity data and emission factors, as detailed in, for example, FOEN (2010) and Heldstab et al. (2016). The two inventories have been designed for the year 2010 and are highly consistent in terms of total emissions over the domain of Zürich. NO$_x$ emissions on the national scale are reported to have decreased by 5–10 % depending on the emission category between 2010 and the period of our simulations. We assume that city emissions follow the national trend and apply corresponding correction factors separately to the individual emission categories.

The UGZ inventory details emissions from thousands of individual sources as line, point or area sources divided into 60 emission categories (cars, motorbikes, gas heating systems, wood heating systems, etc.) within the city limits. Although accounted for in the UGZ inventory, some of these

Table 1. Description of NO_x emission inventories in Zürich as used in GRAL simulations. Emissions inside the limits of the city of Zürich are provided by UGZ, emissions for the rest of the domain by AWEL.

Emission type	Simulated category	Inventory category	Resolution	Total emission ($t\,yr^{-1}/\%$)
Light duty traffic	UGZ light	Cars	7500 lines	495/18.0
		Motorbikes	7500 lines	5.7/2.7
	AWEL light	Cars	15 500 lines	271.6/9.9
		Motorbikes	15 500 lines	4.5/0.2
	AWEL area traffic	Non-road traffic	100 m grid	233.4/8.5
Heavy duty traffic	UGZ heavy	Heavy duty traffic	7500 lines	321.7/11.7
	UGZ bus	Buses	7500 lines	58.9/2.1
	AWEL heavy	Heavy goods vehicles	15 500 lines	154.9/5.6
		Local delivery	15 500 lines	77.8/2.8
	AWEL bus	Local buses	15 500 lines	27.0/1.0
		Long-distance buses	15 500 lines	13.8/0.5
Heating systems	UGZ heating	Oil boilers	10 500 points	251/9.1
		Gas boilers	13 200 points	138/5.0
	UGZ boilers	Hot-water generators	620 points	2.7/0.1
	UGZ wood	Wood-burning systems	900 points	18.7/0.7
	AWEL heating	Oil and/or gas systems	100 m grid	145.0/5.3
	AWEL wood	Wood-burning systems	100 m grid	26.6/1.0
Industry	UGZ industry	Medium-size industries	270 points	29.5/1.1
		Waste-burning and heat plants	56 points	175/6.3
	UGZ off-road	Construction machines	vector areas	75.5/2.8
	AWEL industry	Medium and large industries	100 m grid	86.3/3.1
		Industrial vehicles	100 m grid	100.8/3.7
		Smaller industrial emissions	100 m grid	4.8/0.2
Ships	UGZ ships	Lake-cruise boats	cruise lines	20.9/0.8
	UGZ private boats	Privately owned boats	lake area	5.6/0.2
Total				2744.4/100

emission categories have a very marginal contribution to the NO_x emissions (e.g. forestry and agriculture machines, smokers, animals), or are very punctual (e.g. fireworks), and have therefore been ignored in our simulations. These neglected emissions account for less than 1 % of total NO_x emissions. Individual heating systems are registered by type and size and by the exact location and elevation of the chimney and treated as 26 000 individual point sources. Emissions from cars, motorcycles, lorries and buses are represented as line sources segmented into 5 to 50 m long segments and are based on a comprehensive traffic-emission model and manual traffic-counting campaigns; tunnel portals are modelled as point sources integrating traffic emissions inside the tunnel. The AWEL inventory is less detailed but covers areas that are outside of the city but still inside the GRAL domain. It describes 20 different emission categories as line or area sources. Main roads are described as line sources, while other sources are represented as area sources with a 100 m resolution grid. AWEL emissions are disaggregated to the GRAL grid using the building mask to attribute heating and indus-

trial emissions to building roofs and other emissions to the space between buildings.

As GRAL can account for the rise of hot plumes in ambient air by applying a slightly modified version of the plume-rise model described in Hurley et al. (2005), an initial exhaust temperature and speed is prescribed for point emissions. Such values are available only for the biggest emitters such as waste incineration plants. For all other heating systems, a standard temperature and exhaust speed of 70 °C and $0.8\,m\,s^{-1}$ with a stack diameter of 0.5 m was prescribed. To account for the turbulence induced by the traffic at least to first order, emissions from car and heavy duty traffic are initially mixed within a volume defined by the width of the street (uniformly set at 7 m) and a height of 3 m above street level.

To limit the computational demand, we merged the original categories into a total of 25 group categories by adding up emissions with a similar temporal profile. For instance, we expect motorbike emissions to vary similarly to car emissions. Emission variability in Eq. (1) is determined based on

both pre-defined profiles and measured proxies. For all computed emission categories, we apply typical diurnal, weekly and seasonal cycles as used in the TNO-MACC emission inventory for Europe (Kuenen et al., 2011), with the exception of light duty traffic and heating emissions. A total of 85 traffic counts are operated by the municipality in the city of Zürich. We use the hourly ratios of the total number of vehicles (summed over all sites) to the annual average hourly total. Heating emissions follow a diurnal cycle as prescribed in the TNO-MACC emission inventory, but the seasonal cycle of such emissions is determined using so-called "heating-degree days" accounting for the outdoor temperatures measured at different locations in the city. Heating degree days are computed on the daily scale using Eq. (2):

$$\text{HDD}(t) = \begin{cases} T_{\text{ref}} - T(t) & \text{if } T(t) < T_{\text{min}}, \\ 0 & \text{else} \end{cases} \tag{2}$$

with $T_{\text{ref}} = 20\,°C$, $T_{\text{min}} = 16\,°C$ and $T(t)$ the daily average outdoor temperature in the city at time t.

Heating emissions are scaled proportionally to the heating-degree-days parameter. As the total number of heating degree days varies from one year to another, depending on the meteorology, the scaling factor for heating emissions is chosen to keep consistent heating degree days and emissions for the year 2010 for which the inventory was designed.

3.4 Meteorological and air pollution observations

Meteorological observation sites used for the match-to-observations procedure are shown on the GRAMM domain of Fig. 2. Wherever possible, weather observations are compared with GRAL wind simulations as they are able to represent the influence of nearby obstacles on the air flow. Outside of the GRAL domain, GRAMM mesoscale simulations are used, which limits the selection to standard weather observation sites in open terrain following WMO recommendations as operated by the Swiss Federal Office of Meteorology and Climatology, MeteoSwiss. The remaining weather observations are obtained from air pollution observation sites, maintained by the Swiss national air pollution monitoring network, NABEL; the regional monitoring network for eastern Switzerland, OSTLUFT; and the city environment authority, UGZ. At all MeteoSwiss sites but UEB and LA2, wind speeds and directions are measured on top of a 10 m tall meteorological mast. At UEB and LA2, wind measurements are carried out on top of a 189 and 32 m high telecommunication tower, respectively. Weather observation sites within the city are located above building roofs or in street canyons.

Eight NO_x concentration measurement sites used for evaluating the model are operated within the GRAL domain. GRAL concentrations in the corresponding cells are used for the assessment of the model performance. The rural site TAE, operated by NABEL 25 km away from the GRAL domain boundaries, is taken as regional background site. The site ZUE is located in the centre of Zürich in a courtyard, distant from emission hotspots. The sites BAL, ROS, STA and SCM are located next to busy streets. DUE is operated in the outskirts of the city in a mixed industrial and residential area. HBR is located on the Zürichberg mountain, 200 m above the city centre level, at the limit of the built-up area next to a forest. At all sites, the air inlet is located at 3–4 m a.g.l. NO_x concentrations are measured with standard NO_x monitors: Horiba APNA 360 and Horiba APNA 370. The Horiba APNA instruments use molybdenum converters to convert NO_2 into NO before measuring NO by chemiluminescence. These instruments are therefore also sensitive to other reactive nitrogen compounds, which may lead to some bias in the NO_2 measurements during periods when NO_2 concentrations are low but the concentrations of ozone and other photo-oxidants high (Steinbacher et al., 2007). Such bias are expected to impact significantly the background site TAE as discussed in Sect. 4.2. The instruments are automatically calibrated every 25 h and manually every 2 weeks at NABEL sites, as well as every 10 days at UGZ and OSTLUFT sites. The calibration is carried out through dynamic dilution of a certified NO mixture (Carbagas).

All the sites mentioned above provide continuous hourly measurements for the simulated period from January 2013 to December 2014. The monitoring network is complemented by a network of 65 passive NO_2 samplers maintained by UGZ and OSTLUFT. These samplers are collected every 2 weeks and analysed in the laboratory shortly after collection. For making the biweekly samples comparable to the continuous observations, a few passive samplers are placed next to continuous sites. NO_2 observations from all passive samplers are then corrected with a linear correction function by comparing continuous and passive measurements at these sites.

Temperature data used to scale emissions from heating systems are gathered at the same locations as the wind data. The average outdoor temperature for the entire city is calculated as the mean of available observations. Traffic counts are located all around the city. They count vehicles regardless of their type on a 15 min basis direction-wise for all lanes of selected streets. We use hourly totals in the city to scale traffic emissions uniformly.

4 Results

After generating the catalogue of wind and concentration fields, hourly time series of concentration maps have been generated for the years 2013 and 2014. In the following, these model outputs are evaluated against observations and an analysis of uncertainties of the model system is presented.

Table 2. Model performance for NO_x concentrations at all observation sites on the hourly and daily scales. Ref = standard simulation at the exact location of observation sites. Min = simulated minimum in a radius of 15 m horizontally and 2 m vertically. The score metrics are defined in Sect. 2.3. The left column for each score represents the FAIRMODE performance objective (defined in Sect. 2.3) following Thunis et al. (2012) dependent on U; the right column is the computed score. Values not fulfilling the FAIRMODE objective are reported in bold. Sites are sorted by increasing observed mean.

Temporal scale	Simulation ID	Site ID	Observed mean ($\mu g\,m^{-3}$)	15 m radius range ($\mu g\,m^{-3}$)	NMB (%)		MFB (%)		RPE (%)		FAC2 (%)		r		MQO
Hourly	Ref	HBR	23.1	7.1	46	29	46	30	50	27	50	78	0.66	0.78	0.81
		FIL	38.1	6.6	37	36	37	29	50	36	50	64	0.78	**0.61**	**1.37**
		DUE	45.1	10.3	43	40	43	43	50	33	50	61	0.78	**0.62**	**1.31**
		ZUE	46.6	12.9	42	26	42	28	50	23	50	76	0.68	0.73	0.93
		STA	63.9	30.3	53	29	53	33	50	23	50	73	0.46	0.75	0.68
		BAL	93.5	70.8	77	25	77	9	50	35	50	66	0.0	0.53	0.68
		SCM	95.9	58.7	65	52	65	36	50	**62**	50	68	0.27	0.66	0.80
		ROS	119.8	331.2	69	**135**	69	67	50	**165**	50	**43**	0.23	0.62	**1.07**
		ROS2	119.8	322.7	69	**79**	69	45	50	**102**	50	56	0.0	0.60	0.79
		All	65.3	57.3	106	51	106	33	50	**52**	50	67	0.0	0.67	0.66
	Min	HBR	23.1	7.1	46	8	46	14	50	8	50	85	0.66	0.79	0.78
		FIL	38.1	6.6	37	18	37	18	50	17	50	68	0.78	**0.64**	**1.25**
		DUE	45.1	10.3	43	22	43	31	50	15	50	66	0.78	**0.64**	**1.23**
		ZUE	46.6	12.9	42	−8	42	5	50	−15	50	83	0.68	0.76	0.92
		STA	63.9	30.3	53	−11	53	1	50	−17	50	83	0.46	0.79	0.63
		BAL	93.5	70.8	77	−6	77	−13	50	3	50	62	0.0	0.58	0.53
		SCM	95.9	58.7	65	−4	65	−1	50	−2	50	81	0.27	0.72	0.52
		ROS	119.8	331.2	69	17	69	9	50	31	50	70	0.23	0.58	0.52
		ROS2	119.8	322.7	69	18	69	10	50	32	50	70	0.0	0.58	0.53
		All	65.3	57.3	106	1	106	7	50	−1	50	76	0.0	0.71	0.38
Daily	Ref	HBR	23.1	7.0	39	28	39	32	50	19	50	92	0.60	0.93	0.41
		FIL	36.0	6.1	31	**33**	31	31	50	37	50	80	0.73	0.83	0.79
		DUE	44.6	10.2	36	**40**	36	43	50	25	50	72	0.70	0.85	0.71
		ZUE	46.7	13.0	37	26	37	30	50	21	50	90	0.60	0.87	0.58
		STA	64.0	30.4	46	29	46	32	50	20	50	87	0.20	0.87	0.41
		BAL	93.3	69.8	52	24	52	13	50	39	50	86	0.0	0.70	0.52
		SCM	96.0	58.9	56	52	56	39	50	**60**	50	78	0.0	0.81	0.47
		ROS	119.8	331.7	48	**135**	48	**78**	50	**151**	50	**31**	0.07	0.75	0.78
		All	64.6	56.0	85	51	85	36	50	**63**	50	79	0.0	0.80	0.54
	Min	HBR	23.1	7.0	39	7	39	14	50	1	50	98	0.60	0.93	0.44
		FIL	36.0	6.1	31	15	31	17	50	18	50	88	0.73	0.84	0.76
		DUE	44.6	10.2	36	22	36	31	50	8	50	84	0.70	0.86	0.72
		ZUE	46.7	13.0	37	−7	37	2	50	−15	50	98	0.60	0.88	0.69
		STA	64.0	30.4	46	−11	46	−4	50	−18	50	98	0.2	0.89	0.45
		BAL	93.3	69.8	52	−7	52	−13	50	5	50	88	0.0	0.73	0.39
		SCM	96.0	58.9	56	−4	56	−3	50	−2	50	97	0.0	0.84	0.33
		ROS	119.8	331.7	48	17	48	17	50	14	50	97	0.07	0.74	0.34
		All	64.6	56.0	85	1	85	6	50	2	50	94	0.0	0.86	0.26

4.1 General model performance

Our model is evaluated at all sites against the FAIRMODE performance criteria defined in Sect. 2.3. All FAIRMODE scores are reported in Table 2. In the reference simulation, most sites fulfil the criteria. No more than ∼ 15 % of all computed scores are beyond the FAIRMODE performance criteria. The few exceptions are discussed below.

At the site ROS, the model largely overestimates the concentrations, resulting in poor scores for NMB, FAC2, RPE and MQO. This can be explained by the very steep gradients in the vicinity of the site. ROS is located on a small parking lot, adjacent to the busiest traffic corridor in the city. Simu-

lated concentrations vary spatially by more than 300 $\mu g\,m^{-3}$ within a radius of 15 m around the exact location of the site, compared to the observed average of 120 $\mu g\,m^{-3}$. Small errors in the location of the emissions relative to the site or in the computation of the flow fields have a critical impact on such a site. At the site SCM, the relative percentile error exceeds the requirement threshold due to overestimated concentration peaks. The site SCM is a traffic site similar to ROS, with likely similar reasons for overestimation. However, an overestimation at SCM is only evident for the highest concentrations, whereas at ROS the concentrations are generally too high. The sites FIL and DUE do not fulfil all FAIRMODE performance objectives as well, but in their case this
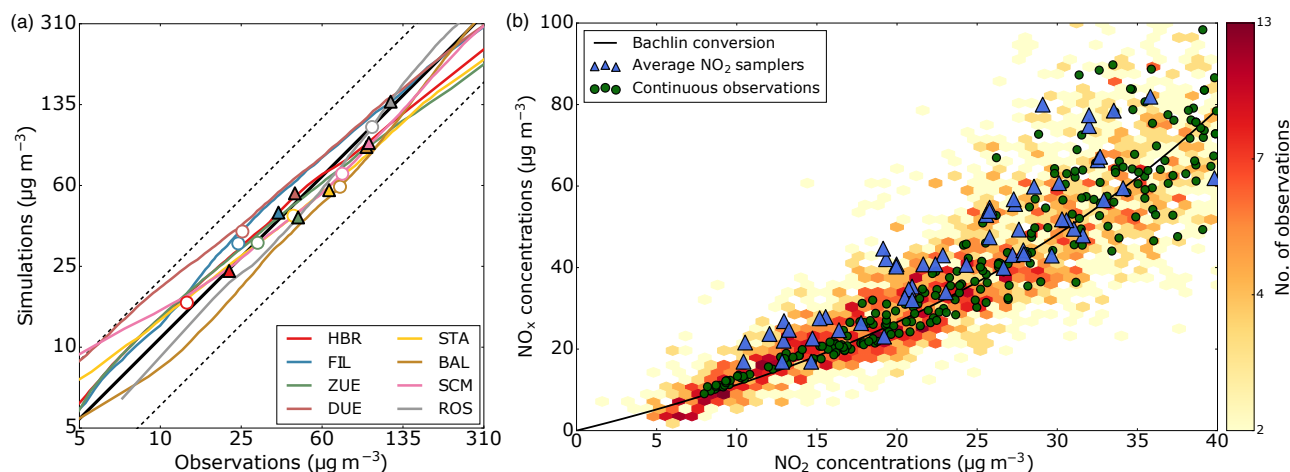
Figure 3. Comparison of observed and simulated NO_x and NO_2 concentrations. **(a)** quantile–quantile plot of hourly NO_x concentrations at continuous sites. The solid and dashed black lines are the 1 : 1 line and the 1 : 2 and 2 : 1 lines, respectively. Filled triangles are the 2013–2014 mean and empty circles the median concentrations. Note the logarithmic scale of the plot. **(b)** Concentrations at passive samplers. Yellow to red coloured background show the comparison between 2-weekly observed NO_2 (x axis) and corresponding simulated NO_x (y axis). Triangles are the mean values per station averaged over the entire period 2013–2014. For comparison, green dots are the 2-weekly averages of NO_2 and NO_x as observed at continuous sites. The black line is a "Bachlin"-type parametrization of the ratio between NO_x and NO_2 (Düring et al., 2011).

is due to insufficient correlation between observations and simulations on the hourly scale. The site DUE is located in an industrial area, next to a busy highway, while FIL is located in a rural environment but next to a motorway intersection and the portals of the three tunnels of the motorway bypass in Zürich West. Incorrectly prescribed variability in related traffic and industrial emissions may explain the insufficient scores. Discrepancies between observations and simulations are further discussed in the following sections to identify error sources and propose possible model improvements.

Though fulfilling the quality objectives in most cases, the modelling system seems to generally overestimate concentrations at all observation locations. The overestimation might be attributed to incorrect emission magnitude in the inventories. However, when considering the minimum values within a 15 m horizontal and 2 m vertical distance, all performance scores at all sites are significantly improved. The biases almost vanish and the synthesis MQO index is smaller than 1 at almost all sites on the hourly and daily scale, and even below 0.5 on average. A MQO below 0.5 was considered by Thunis et al. (2012) as a reference objective since observation errors start dominating model error below 0.5. The general improvement of the model performance when taking the minimum in a certain distance rather than values at the exact location of the observations suggests that the dispersion of pollutants is generally underestimated, especially in the vicinity of emission hotspots. In fact, GRAL is known for overestimating pollutant concentrations near building façades (Oettl, 2015b). In addition, traffic-induced turbulence is accounted for only by spreading traffic emissions over the lowest 3 m above ground (see Sect. 3.3). The

better performance of the model in the minimum simulation at traffic sites suggests that additional efforts should be made to better parametrize the traffic-induced turbulence.

The temporal correlations between simulations and observations do not change drastically between the two approaches, but for this metric there is also an improvement when using the minimum values in most cases. The correlations between observations and simulations are in the range 0.53–0.79 on the hourly scale and 0.71–0.94 on the daily scale. At most sites, these correlations are at least 0.5 higher than the correlations between observations and temporally varying emissions, which demonstrates that meteorological variability is a key factor driving the variability in concentrations and that this variability is very well captured by the catalogue-based modelling approach. Exceptions are the sites ROS, SCM and BAL for which the correlations are only 0.05 to 0.2 better than the emission–observation correlations. At these traffic sites the variability appears to be dominated by traffic intensity rather than by meteorology.

In the following, we compare observations to the "minimum" simulations due to their significantly better performance, and will further discuss the implications of this choice in Sect. 5.

4.2 Evaluation of the spatial distribution

The average distribution of simulated NO_x concentrations is shown in Fig. 2. Apart from hills and forest areas, where the concentrations are close to the background, NO_x concentrations are dominated by local emissions in most built-up areas. Large gradients exist between traffic corridors with con-

centrations higher than $100 \, \mu g \, m^{-3}$ as well as backyards and smaller streets.

To evaluate the quality of this average distribution, we use 8 continuous monitoring sites and 65 NO_2 passive samplers distributed rather uniformly over the city and covering the full range of pollution levels. Figure 3 and Table 2 compare average observations with simulations. As shown by the quantile–quantile plot and the biases, there is no specific dependency of the mismatches on the concentrations. The fractional bias remains roughly the same (well below 50 %) at all sites over the whole range of observed concentrations. As for the biases, it is considered that an air pollution model is performing well when the NMB is below 50 % (e.g. Kumar et al., 2006). The relative bias only seems to increase at all sites at the lower and upper end of the concentration range, suggesting higher uncertainties for very high and very low concentrations.

At passive sampler sites the comparison is complicated by the fact that the modelling system simulates NO_x, whereas passive samplers measure NO_2. The ratio between NO_2 and NO_x is often parametrized by a non-linear "Bachlin" function depending solely on the concentration of NO_x (e.g. Düring et al., 2011). The function accounts for the fact that the ratio tends to increase with increasing distance from the source and hence with decreasing NO_x concentration. The ratios between biweekly averaged NO_2 and NO_x concentrations measured at the continuous sites (green dots in Fig. 3) indeed closely follow a Bachlin curve, though with increasing spread at high NO_x concentrations. The ratios between the 2-year averages of NO_2 measured at the passive samplers and the corresponding simulated NO_x values follow this curve as well, although the simulated NO_x values tend to be somewhat too high. For the individual 2-weekly averages (coloured background in Fig. 3b), this overestimation is particularly evident for the low concentrations. These low concentrations mainly occur during the summer season when the lifetime of NO_x is shortest. The overestimation of low concentrations could therefore be a result of treating NO_x as a passive tracer in the model, not accounting for photochemical depletion. Furthermore, Steinbacher et al. (2007) demonstrated that NO_x concentrations at TAE, which are added as a background to our simulations, are generally overestimated by $3–4 \, \mu g \, m^{-3}$ due to interferences of other reactive nitrogen compounds like PAN and HNO_3 when using a molybdenum converter.

Apart from a possible overestimation of very low concentrations, our modelling system is able to reproduce the large spatial variations in average concentration levels with high confidence.

4.3   Evaluation of the temporal variability

Good scores for the average spatial distribution of air pollutant concentrations have already been demonstrated for other modelling systems (e.g. Soulhac et al., 2011; Di Sabatino et al., 2007). However, accurately reproducing not only average concentrations but also the temporal evolution from hourly to seasonal timescales is a much more challenging objective that has received little attention so far. This section therefore focusses on evaluating the simulated temporal variability.

4.3.1   Example period

In Fig. 4, observations are compared to simulations for a selected period of time, October 2013. The period has been selected as it is the only time that all sites were in operation, but also because the concentrations represented the average patterns of concentration variability rather than some specific pollution events. The simulations are divided into their main contributors (background, light and heavy duty traffic, heating systems and the rest). Sites are sorted following the average observed NO_x concentrations, from the highest at ROS to the lowest at HBR. Simulations at all sites are generally in very good agreement with observations: the diurnal cycle is mostly well reproduced and the different concentration patterns during weekends (shaded periods in Fig. 4) are well detected. Whereas background concentrations are the same at all sites and never exceed $50 \, \mu g \, m^{-3}$, the magnitude of local contributions varies significantly from one site to the other, very consistently with observations. FIL and HBR show almost no local contribution, whereas street sites such as ROS and SCM are largely dominated by local traffic emissions. However, at the three most polluted sites, ROS, SCM and STA, the simulations deviate significantly from the observations for some periods. As discussed earlier this is likely related to the large local gradients at these sites of 30, 59 and $330 \, \mu g \, m^{-3}$ on average within a distance of 15 m at STA, SCM and ROS respectively.

At all sites, traffic emissions are the biggest contributor to air pollution. Since the variability of traffic emissions does not change significantly from one day to the next (apart from the weekends), most of the concentration variability is attributable to changes in weather conditions, and this variability is generally well captured by the simulations. For instance, four events with strong winds (see wind speed in the upper panel of Fig. 4) and correspondingly low concentrations are well reproduced. Nevertheless, inconsistencies in the selection of weather situations occasionally appear, as suggested by sporadic peaks mostly at the site DUE, which appear in the simulations but not in the observations. Such events are not realistic most of the time and could point at a too-frequent selection of very stable situations by the match-to-observation procedure. Such peaks may be amplified through the catalogue-based procedure, since particles emitted during a 1 h time span are fully attributed to the same hour in the steady-state assumptions, while some particles are transported longer than 1 h. Still, a few short peaks are observed and reproduced, demonstrating the ability of the system to capture short-term changes in weather conditions.
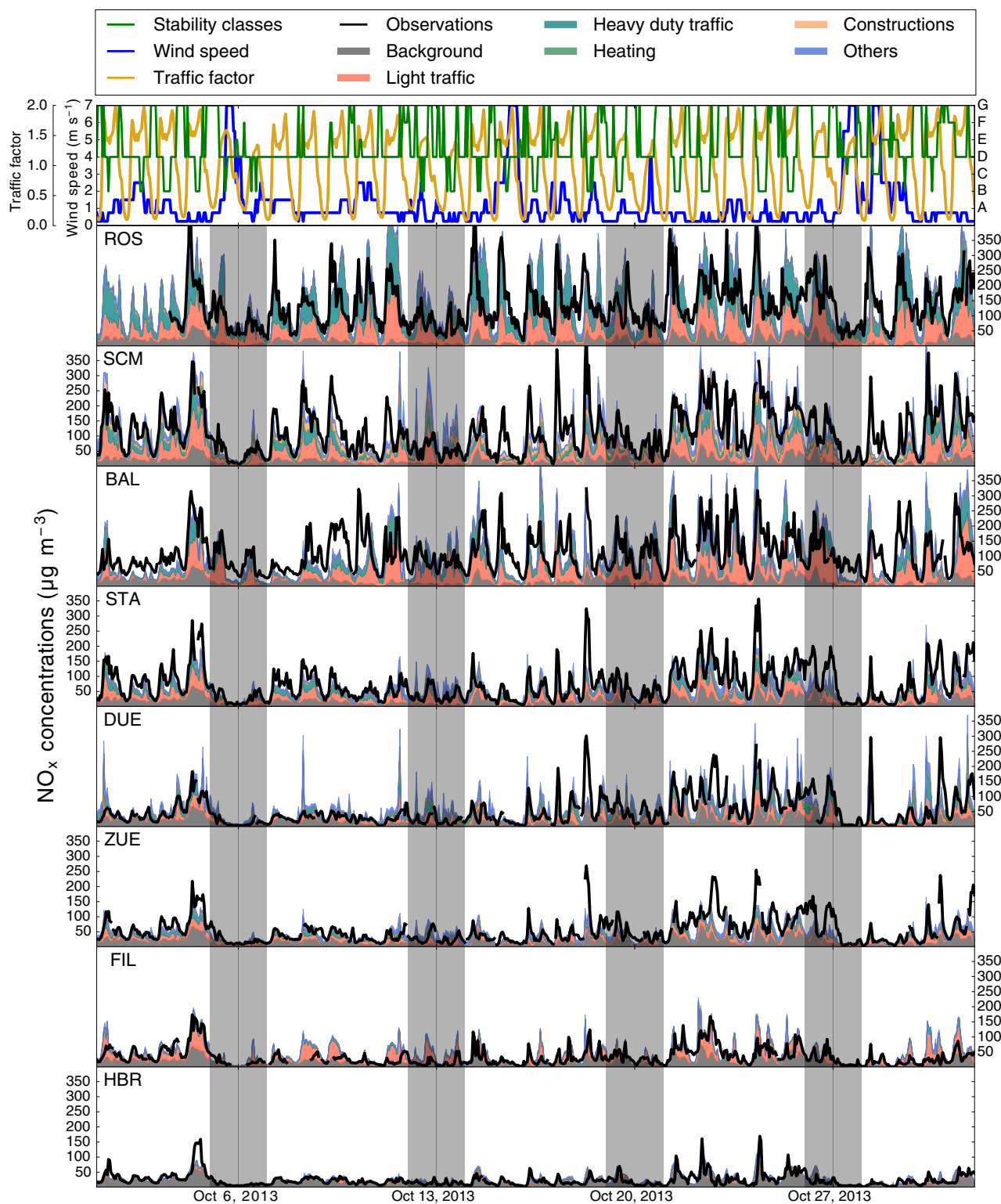
Figure 4. Hourly time series of observed and simulated concentrations at all sites for the month of October 2013. Simulations are separated by contributions from the main emission categories (light traffic, heavy duty traffic, heating and the rest). Shaded periods represent weekends. Top: stability classes and wind categories of the hourly selected weather situations.
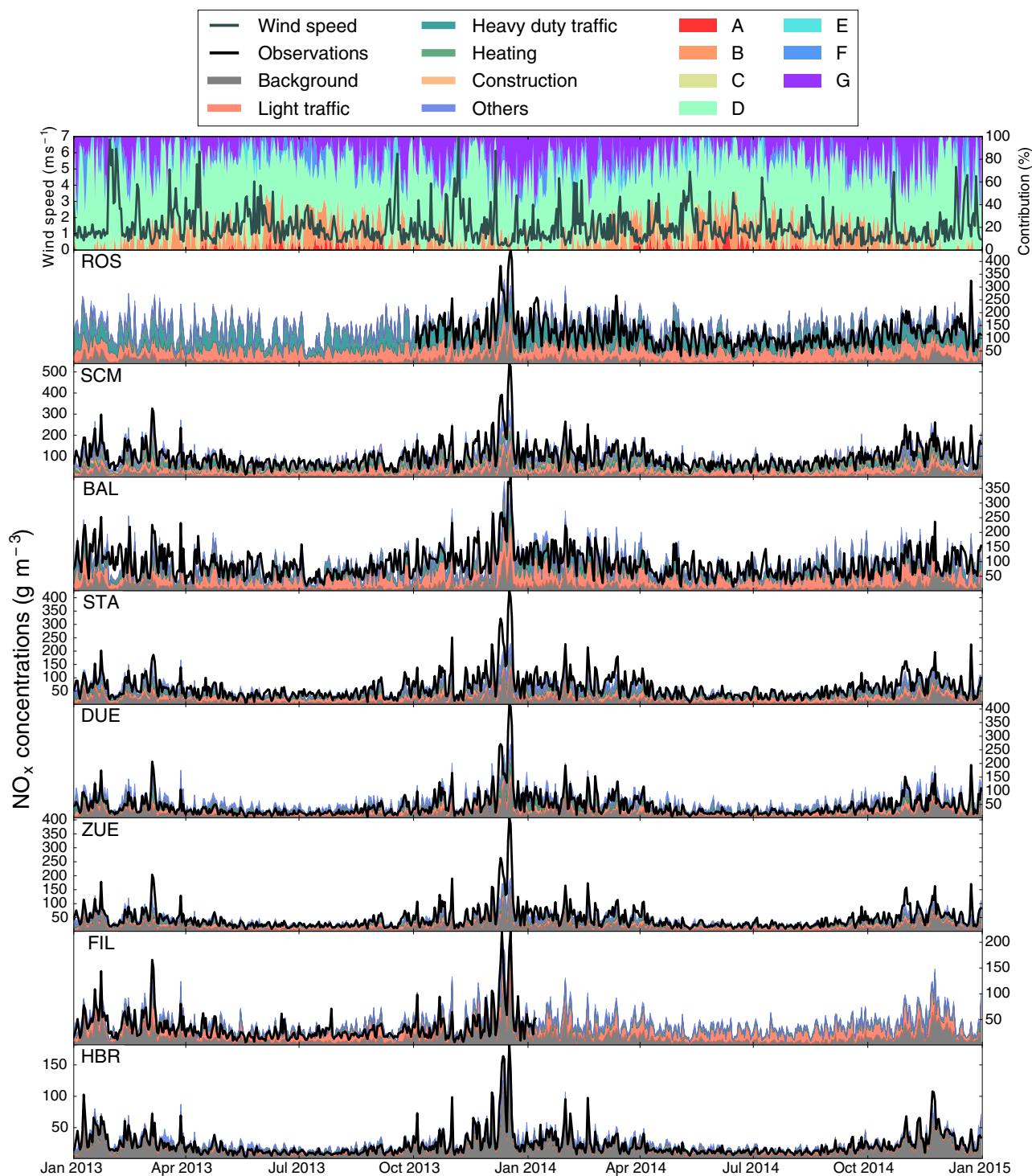
Figure 5. Daily observed and simulated concentrations at all observation sites for the years 2013 and 2014. Simulations are separated by contributions as in Fig. 4. Top: daily averages of stability class contributions (A–G) and wind categories. Measurements at FIL were discontinued in January 2014, whereas the site ROS started being operated in October 2013.

At the site HBR, 200 m above the altitude of the city centre, the concentrations are dominated by the background and are in most cases well reproduced. However, in some very specific situations, the modelling system appears to miss some transport of pollution from the valley to higher altitudes. For instance, a pollution event was observed at all sites

on 4 October in Fig. 4. It was well reproduced by the model at all sites with the exception of HBR, where the model only marginally deviated from the background, suggesting underestimated vertical transport from the city centre, or a mismatch in simulated wind directions at higher altitudes.

4.3.2 Complete 2-year period

The entire period of simulation, covering the years 2013 and 2014, is presented in Fig. 5, similar to Fig. 4 but with daily instead of hourly averages. Synoptic variability characterized by periods of strong air pollutant accumulation alternating with cleaner periods is superimposed on a seasonal cycle with systematically higher concentrations during winter. The synoptic variability, which is manifested by varying contributions from emissions within the city with changing weather conditions, is very well reproduced with good FAC2 scores and high correlation coefficients for daily averages ($r = 0.86$ on average; see Table 2). At all sites, FAC2 and r scores are 10–20 % higher on the daily scale than on the hourly scale, indicating that the synoptic variability is better captured than the diurnal cycle. Events of low concentrations are generally correlated with higher wind speeds, whereas concentration peaks are associated with particularly stable situations (stability classes E to G).

Although heating systems dominantly emit during wintertime, they contribute only marginally to the seasonal cycle of concentrations simulated by the system. Indeed, all the observation sites are located close to the ground at 3–4 m, while heating emissions occur on building roofs and rise further after release, thus impacting ground concentrations only a little. The seasonal cycle of NO_x concentrations is, thus, mostly driven by the vertical stability of the atmosphere rather than by the seasonal cycle of emissions. Convective situations are more frequent and pollutants are therefore mixed more effectively during summer, reducing ground concentrations, whereas they accumulate close to the surface in winter. Because of increased stable conditions, NO_x pollution events tend to be more severe in winter at all sites. Therefore, the background concentrations partly explain the seasonal cycle of city concentrations, especially in the background site HBR and during the strong pollution event in December 2013. Local contributions from traffic emissions dominate the seasonal variability at all other sites even though traffic emissions do not change significantly from one month to another.

In December 2013, a particularly strong pollution event occurred. During this month, observed daily averages reached up to 700 µg m^{-3}, with values above 200 µg m^{-3} at all sites. These very high concentrations are explained by the combination of regional recirculation of pollution (average background concentrations were 48 µg m^{-3} for this month), low winds and highly stable conditions enhancing the urban contribution. The modelling system reasonably fills the gap between observed peaks and the background. However, it is unable to reach the observed peak concentrations at most sites. The accumulation of pollutants in the city likely occurred over a timescale of several hours, which our approach with steady-state hourly simulations is unable to reproduce. This approach underestimates air pollutant accumulation within the city during periods of particularly low wind speeds, since this local accumulation cannot be represented by the rural background and as particles crossing the domain borders cannot re-enter the limited-area domain. General improvements in the model set-up (e.g. higher spatial and temporal resolution and a bigger domain) as well as in the method (temporal hysteresis from one hour to the next) will be needed to better reproduce such severe pollution events.

Figure 6 presents a general temporal evaluation (RMSEs and correlation coefficients) of the model at all passive samplers. Biweekly NO_2 observations are compared to the corresponding NO_2 values from the model obtained using the NO_x-to-NO_2 conversion formula of Düring et al. (2011) (black line in Fig. 3). For reference, correlation coefficients and RMSEs have been calculated as well for different concentration intervals based on biweekly averages from continuous measurements of NO_2 and NO_x, represented by the blue and green line in Fig. 6, respectively. These lines, which are only based on observations, provide a measure of the uncertainties implied by the NO_x–NO_2 conversion alone and therefore of the best score achievable by the model. It appears that the 2-weekly correlation coefficients are very similar to the uncertainties implied by the conversion, suggesting a very good agreement between observations and simulations, in agreement with the high correlations for the daily averages at the continuous sites in Table 2. The RMSEs are on average 2 times larger (3 µg m^{-3}) than the conversion uncertainties. Contrary to RMSEs computed from continuous sites, RMSEs from converted simulations at passive sites do not show any clear dependency on concentration levels. This may partly be attributable to the systematic bias at the background site TAE for low concentrations (see Sect. 4.2).

4.3.3 Diurnal cycle of concentrations

Beyond the seasonal and daily variability, the diurnal cycle of concentrations plays a key role in assessing the exposure of the population to air pollution as people commute and spend their day at different locations within the city. The mean diurnal cycles of observations and simulations are presented in Fig. 7. Here, only weekdays are discussed as the diurnal cycle of emissions is more pronounced than during weekends. Consistent with the observations, the simulated concentrations are higher at daytime than during the night, with a morning peak at all sites and a late afternoon peak at some sites.

The morning rush hour leads to a stronger peak as the atmosphere is usually more stably stratified at this time of the day than during the evening rush hour. At most sites, both in the model and the observations, the peak occurs at
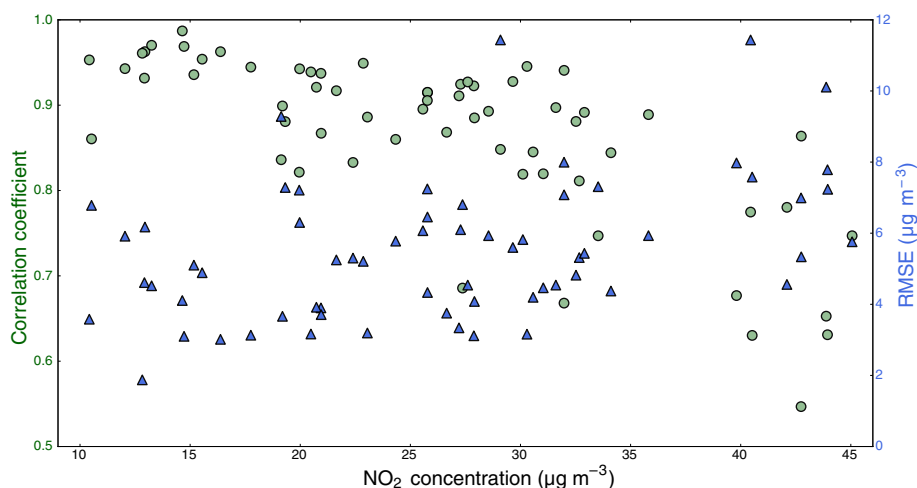
Figure 6. Correlation coefficients (green dots) and RMSE (blue triangles) at all passive samplers as a function of the mean NO_2 concentration at each site for the 2-year period 2013–2014. NO_x simulations are converted to NO_2 using the parametrized conversion of Düring et al. (2011). The green and blue line corresponds to the correlation coefficient and RMSE, respectively, computed for $5\,\mu g\,m^{-3}$ wide sliding concentration intervals by comparing 2-week averages of continuous NO_2 observations with converted equivalents of observed NO_x.
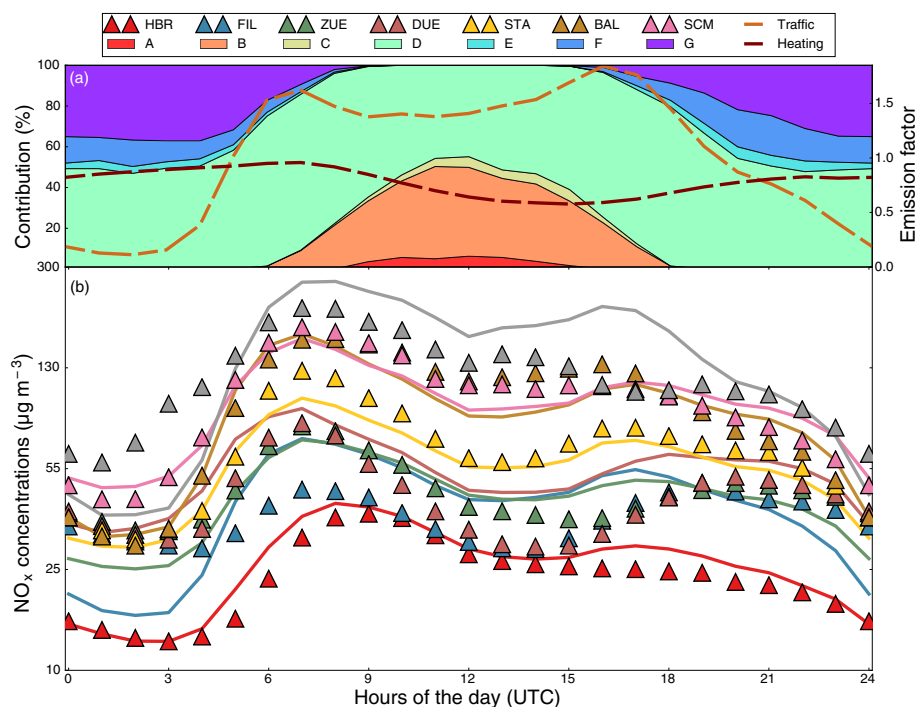
Figure 7. A 2-year mean diurnal cycle of concentrations, traffic emissions and meteorology during weekdays. **(a)** Contributions of stability classes (A: very unstable; D: neutral; G: very stable) to the hourly meteorology. The dashed lines are the emission profiles for light traffic and heating emissions. **(b)** Diurnal cycle of observed (triangles) and simulated NO_x concentrations (solid lines) at continuous measurement sites.

07:00 UTC, which corresponds to 08:00 UTC in winter and 09:00 UTC in summer. At HBR, the simulated and observed peaks happen later than at other sites. However, the observed peak is delayed by about 1 h more than the simulated one. As mentioned in Sect. 4.3.1, HBR is an elevated site with no significant emissions nearby. Thus, pollution emitted in the morning in the city appears to be transported to the site with a delay of 2–3 h, while in the model, the steady-state assumption makes pollutants appear to be transported virtually faster.

After the morning peak, the observed concentrations follow three possible paths: a steady decrease until the nighttime minimum (ROS, SCM, HBR), an afternoon plateau with a small peak around 16:00 UTC (STA, BAL) at the same time as the afternoon traffic peak, or a plateau with a late-evening concentration peak around 20:00–21:00 UTC (FIL, DUE, ZUE). These patterns are correctly reproduced by the model at the sites HBR, BAL, STA and DUE. At the other sites, the model simulates an afternoon plateau followed by a small peak from traffic contributions not consistent with observations. The uniform scaling of traffic emissions is a strong simplification that likely contributes to the discrepancies between simulated and observed diurnal profiles at some sites: a closer analysis of the data from the 89 traffic counters, for example, showed that the traffic intensity remains constantly high at daytime in the city centre, whereas there are clear morning and evening peaks in the outer districts. In addition, some streets are more intensively used by incoming traffic (strong morning peak), others by outgoing traffic (strong evening peak). The late-evening peak at 20:00–21:00 UTC could be explained by late emissions such as a surge in domestic heating before the night not accounted for in our system. A second explanation for the absence of a late-evening peak in the simulations could be twofold: first, NO_x is transported in the model as a passive tracer, whereas in reality it is depleted by reaction with OH radicals. OH concentrations are highest when NO_x is relatively low and solar radiation large (Ren et al., 2003), i.e. on sunny summer afternoons. The NO_x lifetime is then reduced to about 2–4 h (e.g. Liu et al., 2016), and not accounting for this depletion will contribute to a positive model bias in the afternoon as seen especially at sites in the lower range of the concentration levels. Second, the observed late-evening peak occurs well after the evening rush hour, suggesting that it is an integrated response due to accumulation of NO_x over several hours. Such effects are not represented by our steady-state approach where the concentrations are solely determined by the emissions of the actual hour.

During the night, observed concentrations at the sites BAL, DUE, ZUE, FIL and STA converge to a similar level, which is well reproduced by the model at BAL, DUE and STA, but underestimated at ZUE and especially at FIL. A systematic underestimation at night is also observed at ROS, especially in the early morning hours. The sites ROS and FIL are located next to important traffic corridors which might be used during the night more heavily than other roads including heavy duty traffic. Heavy duty traffic is not allowed in Switzerland at night between 22:00 and 05:00 LT (20:00–03:00 UTC in summer) but uses the early morning before the main rush hour intensively. Therefore, heavy duty traffic emissions close to these sites might be underestimated in our system. A second explanation can also be the missing accumulation of pollutants at night, similar to the late-evening peak. Under stable nocturnal situations, pollutants are slowly dispersed and remain longer in the domain of simulation than during the day. Accounting for air pollution accumulation over more than 1 h would help increase the nocturnal low concentrations.

5 Discussion and conclusions

A catalogue-based approach computed with the nested simulation system GRAMM–GRAL was applied to simulating hourly NO_x concentration maps at 10 m resolution for the years 2013–2014. The modelling system was evaluated with 8 continuous NO_x measurements sites and 65 NO_2 passive sampler sites. The overall model performance was compliant with the objective criteria of the European air quality modelling framework FAIRMODE on both the hourly and the daily scale for most stations. The temporal variability of concentrations was well reproduced on the hourly, daily, 2-weekly and seasonal scales. This can be explained to a minor extent by the proper representation of the variability in emissions, especially on the diurnal timescale, but it is mostly due to the successful representation of the meteorological variability by the catalogue-based approach. The diurnal cycle of concentrations, which is particularly critical to reproduce the pollution exposure of individuals commuting in the city, is largely consistent with the observations despite a systematic underestimation of concentrations during the night at some locations. The generally good performance of our system, on top of the reasonable computation costs and its flexibility (making it possible to carry out numerous simulation scenarios as it was done in Berchet et al., 2017b), makes it a very suitable solution for designing informed air quality plans urgently needed on the city scale (Miranda et al., 2015).

Recent progress in parametrized approaches allows standard urban air pollution models to reach performances on the yearly or even monthly scale (e.g. ADMS-urban system; Dedele and Miskinyte, 2015) comparable to our approach. The model accuracy on diurnal to daily timescales, however, has hardly ever been analysed, which makes it very difficult to place our results in context but also demonstrates the uniqueness of the simulations presented in this work. On shorter temporal scales, our modelling system is still out-performed by very high-resolution CFD models (Kumar et al., 2015a), but these systems are limited to small domains and short periods of time. Less complex systems such as SIRANE (Soulhac et al., 2012), solving the high-resolution flow only in street canyons and approximating the dispersion above the urban canopy as Gaussian plumes, perform similarly to our model, albeit at higher computational costs, limiting their application to periods of typically a few weeks only. Despite the usage of an extremely detailed emission inventory, our simulations are still significantly limited by the representation of emissions, since only standard temporal profiles were applied to most sources, which are unable to capture the large temporal dynamics of real emissions. Real-time emission models, accounting for the influence of

actual activities such as traffic density and energy consumption or environmental factors such as outdoor temperature affecting not only heating (whose intensity is already modulated by temperature in our model through heating-degree days) but also cold-start traffic emissions (as suggested by the Handbook of Emission Factors for Road Transport v3.3; Keller et al., 2017), could further advance the representation of emissions variability in the future. Such emission models and complementary influence on emission variability could be informed for instance by mobile-phone data and sensor networks. Such improved inputs proved to significantly increase the performance in other models (e.g. Soulhac et al., 2012; Borrego et al., 2016). The main gain of the catalogue-based method is, above all, the reduced computational cost allowing for high-resolution simulations of long time periods with a time resolution down to 1 h. Further developments are required to improve this approach by replacing fixed emission patterns with transient ones, obtained for instance with suitable traffic models.

A general overestimation of concentrations was found at all sites in our model, mostly related to insufficient dispersion in the model as well as to unrealistic accumulation of pollutants near building façades, which have a strong impact on simulations with the chosen 10 m horizontal resolution. The apparently too-low dispersion may be related to the fact that traffic-induced turbulence is only crudely represented. Some limitations of the catalogue-based method were revealed, which are attributable to the steady-state assumption and the limited model domain. Particles that have been transported in the city for more than an hour are assigned to the same hour they were released in the current version of the system. Future versions should account for the particle transport age, which can be made accessible in the GRAL model outputs. This would likely smooth out some of the unrealistic short peaks produced in our simulations. A long residence time of particles in the simulation domain can also have implications in terms of chemistry. NO_x depletion due to oxidation by OH radicals or night-time N_2O_5 chemistry was neglected in our system, as the typical lifetime of NO_x in the atmosphere is never shorter than a few hours (during sunny summer afternoons; Liu et al., 2016). Accounting for long residence times in the simulation domain may allow us to compute simplified chemical reactions within the framework of the catalogue-based approach.

As demonstrated in this study, our model system produces a very realistic representation of the spatial distribution and temporal variability of NO_x in the city, which makes it a highly suitable tool for policy makers. The city of Zürich is indeed implementing the system as a new tool for improved air pollution control and urban planning. So far, our simulations have been generated without any input from actual air pollution measurements. Incorporating such observations through data assimilation and machine learning methods could further enhance the quality of the model predictions and satisfy the requirements of epidemiological stud-

ies even more, which need to be based on accurate, unbiased data. The selection of weather situations in the catalogue could also benefit from assimilating concentration observations in the system, instead of wind and radiation observations only. Additional meteorological observations not directly related to the definition of the catalogue, such as turbulence fluxes, temperature gradients or boundary layer height, are also increasingly available and might improve the selection of weather situations in the catalogue as well. A fully integrated high-resolution modelling system would enable short- and long-term pollutant and greenhouse gas monitoring in cities for subsequent use in the development of mitigation strategies.

Finally, NO_x concentrations are relevant for regulation purposes only as a proxy of NO_2 concentrations. Oettl and Uhrner (2011) introduced a chemical module to GRAL, but the transient-based approach of this module with explicit computation of O_3 three-dimensional fields prevents the benefit of the reduced computation costs of the catalogue-based approach. An intermediate system, accounting for the average distribution of particle age and rough estimates of O_3 concentrations, should be tested in future to reproduce NO_2 concentrations on fine scales in cities.

References

Almbauer, R. A., Oettl, D., Bacher, M., and Sturm, P. J.: Simulation of the air quality during a field study for the city of Graz, Atmos. Environ., 34, 4581–4594, https://doi.org/10.1016/S1352-2310(00)00264-8, 2000.

Anfossi, D., Alessandrini, S., Trini Castelli, S., Ferrero, E., Oettl, D., and Degrazia, G.: Tracer dispersion simulation in low wind speed conditions with a new 2D Langevin equation system, Atmos. Environ., 40, 7234–7245, https://doi.org/10.1016/j.atmosenv.2006.05.081, 2006.

Beelen, R., Hoek, G., van den Brandt, P. A., Goldbohm, R. A., Fischer, P., Schouten, L. J., Jerrett, M., Hughes, E., Armstrong, B., and Brunekreef, B.: Long-term effects of traffic-related air pollution on mortality in a Dutch cohort (NLCS-AIR study), Environ Health Persp., 116, 196–202, https://doi.org/10.1289/ehp.10767, 2008.

Beelen, R., Voogt, M., Duyzer, J., Zandveld, P., and Hoek, G.: Comparison of the performances of land use regression modelling and dispersion modelling in estimating small-scale variations in long-term air pollution concentrations in a Dutch urban area, Atmos. Environ., 44, 4614–4621, https://doi.org/10.1016/j.atmosenv.2010.08.005, 2010.

Beelen, R., Hoek, G., Vienneau, D., et al.: Development of NO_2 and NO_x land use regression models for estimating air pollution exposure in 36 study areas in Europe – the ESCAPE project, Atmos. Environ., 72, 10–23, https://doi.org/10.1016/j.atmosenv.2013.02.037, 2013.

Beelen, R., Raaschou-Nielsen, O., Stafoggia, M., et al.: Effects of long-term exposure to air pollution on natural-cause mortality: an analysis of 22 European cohorts within the multicentre ESCAPE project, Lancet, 383, 785–795, https://doi.org/10.1016/S0140-6736(13)62158-3, 2014.

Berchet, A., Zink, K., and Brunner, D.: Python interface for GRAMM/GRAL modelling system, Zenodo, https://doi.org/10.5281/zenodo.840843, 2017a.

Berchet, A., Zink, K., Muller, C., Oettl, D., Brunner, J., Emmenegger, L., and Brunner, D.: A cost-effective method for simulating city-wide air flow and pollutant dispersion at building resolving scale, Atmos. Environ., 158, 181–189, https://doi.org/10.1016/j.atmosenv.2017.03.030, 2017b.

Borrego, C., Amorim, J. H., Tchepel, O., Dias, D., Rafael, S., Sá, E., Pimentel, C., Fontes, T., Fernandes, P., Pereira, S. R., Bandeira, J. M., and Coelho, M. C.: Urban scale air quality modelling using detailed traffic emissions estimates, Atmos. Environ., 131, 341–351, https://doi.org/10.1016/j.atmosenv.2016.02.017, 2016.

Brandt, J., Silver, J. D., Christensen, J. H., Andersen, M. S., Bønløkke, J. H., Sigsgaard, T., Geels, C., Gross, A., Hansen, A. B., Hansen, K. M., Hedegaard, G. B., Kaas, E., and Frohn, L. M.: Contribution from the ten major emission sectors in Europe and Denmark to the health-cost externalities of air pollution using the EVA model system – an integrated modelling approach, Atmos. Chem. Phys., 13, 7725–7746, https://doi.org/10.5194/acp-13-7725-2013, 2013.

Briant, R., Seigneur, C., Gadrat, M., and Bugajny, C.: Evaluation of roadway Gaussian plume models with large-scale measurement campaigns, Geosci. Model Dev., 6, 445–456, https://doi.org/10.5194/gmd-6-445-2013, 2013.

Brunekreef, B. and Holgate, S. T.: Air pollution and health, Lancet, 360, 1233–1242, https://doi.org/10.1016/S0140-6736(02)11274-8, 2002.

Cohen, A. J., Anderson, H. R., Ostro, B., Pandey, K. D., Krzyzanowski, M., Künzli, N., Gutschmidt, K., Pope III, C. A., Romieu, I., Samet, J. M., and Smith, Kirk R.: Urban air pollution, Comparative Quantification of Health Risks, 2, 1353–1433, http://cdrwww.who.int/publications/cra/chapters/volume2/1353-1434.pdf, 2004.

Dedele, A. and Miskinyte, A.: The statistical evaluation and comparison of ADMS-Urban model for the prediction of nitrogen dioxide with air quality monitoring network, Environ. Monit. Assess., 187, 578, https://doi.org/10.1007/s10661-015-4810-1, 2015.

Di Sabatino, S., Buccolieri, R., Pulvirenti, B., and Britter, R.: Simulations of pollutant dispersion within idealised urban-type geometries with CFD and integral models, Atmos. Environ., 41, 8316–8329, https://doi.org/10.1016/j.atmosenv.2007.06.052, 2007.

Di Sabatino, S., Buccolieri, R., and Salizzoni, P.: Recent advancements in numerical modelling of flow and dispersion in urban areas: a short review, Int. J. Environ. Pollut., 52, 172–191, https://doi.org/10.1504/IJEP.2013.058454, 2013.

Düring, I., Bächlin, W., Ketzel, M., Baum, A., Friedrich, U., and Wurzler, S.: A new simplified NO/NO_2 conversion model under consideration of direct NO_2-emissions, Meteorol. Z., 20, 67–73, https://doi.org/10.1127/0941-2948/2011/0491, 2011.

Duvall, R. M., Long, R. W., Beaver, M. R., Kronmiller, K. G., Wheeler, M. L., and Szykman, J. J.: Performance evaluation and community application of low-cost sensors for ozone and nitrogen dioxide, Sensors, 16, 1698, https://doi.org/10.3390/s16101698, 2016.

EC: Directive 2008/50/EC of the European Parliament and of the Council of 21 May 2008 on ambient air quality and cleaner air for Europe, Tech. rep., Official Journal L 152, available at: http://ec.europa.eu/environment/air/quality/legislation/existing_leg.htm, 2001.

FOEN: Pollutant Emissions from Road Transport, 1990 to 2035, Tech. Rep., Federal Office for the Environment, Bern, available at: http://www.bafu.admin.ch/publikationen/publikation/01565/index.html?lang=en, 2010.

Gao, Y., Dong, W., Guo, K., Liu, X., Chen, Y., Liu, X., Bu, J., and Chen, C.: Mosaic: a low-cost mobile sensing system for urban air quality monitoring, in: IEEE INFOCOM 2016 – The 35th Annual IEEE International Conference on Computer Communications, 1–9, https://doi.org/10.1109/INFOCOM.2016.7524478, 2016.

Hasenfratz, D., Saukh, O., Walser, C., Hueglin, C., Fierz, M., Arn, T., Beutel, J., and Thiele, L.: Deriving high-resolution urban air pollution maps using mobile sensor nodes, Pervasive Mob. Comput., 16, 268–285, https://doi.org/10.1016/j.pmcj.2014.11.008, 2015.

Heimann, I., Bright, V. B., McLeod, M. W., Mead, M. I., Popoola, O. A. M., Stewart, G. B., and Jones, R. L.: Source attribution of air pollution by spatial scale separation using high spatial density networks of low cost air quality sensors, Atmos. Environ., 113, 10–19, https://doi.org/10.1016/j.atmosenv.2015.04.057, 2015.

Heldstab, J., Leippert, F., Wuethrich, P., and Kuenzle, T.: NO$_2$ ambient concentrations in Switzerland. Modelling results for 2005, 2010, 2015, Tech. Rep. 1123, Federal Office for the Environment, Bern, Switzerland, available at: http://www.bafu.admin.ch/publikationen/publikation/01634/index.html?lang=en, 2011.

Heldstab, J., Schaeppi, B., Weber, F., and Sommerhalder, M.: Switzerland's Informative Inventory Report, Tech. Rep., Federal Office for the Environment, Bern, available at: http://www.bafu.admin.ch/luft/11017/11024/11592/index.html?lang=de&download=NHzLpZeg7t, lnp6I0NTU042l2Z6ln1acy4Zn4Z2qZpnO2Yuq2Z6gpJCGeoN_e2ym162epYbg2c_JjKbNoKSn6A--, 2016.

Hurley, P. J., Physick, W. L., and Luhar, A. K.: TAPM: a practical approach to prognostic meteorological and air pollution modelling, Environ. Modell. Softw., 20, 737–752, https://doi.org/10.1016/j.envsoft.2004.04.006, 2005.

Jerrett, M., Arain, A., Kanaroglou, P., Beckerman, B., Potoglou, D., Sahsuvaroglu, T., Morrison, J., and Giovis, C.: A review and evaluation of intraurban air pollution exposure models, J. Expo. Anal. Env. Epid., 15, 185–204, https://doi.org/10.1038/sj.jea.7500388, 2004.

Jiao, W., Hagler, G., Williams, R., Sharpe, R., Brown, R., Garver, D., Judge, R., Caudill, M., Rickard, J., Davis, M., Weinstock, L., Zimmer-Dauphinee, S., and Buckley, K.: Community Air Sensor Network (CAIRSENSE) project: evaluation of low-cost sensor performance in a suburban environment in the southeastern United States, Atmos. Meas. Tech., 9, 5281–5292, https://doi.org/10.5194/amt-9-5281-2016, 2016.

Kakosimos, K. E., Hertel, O., Ketzel, M., and Berkowicz, R.: Operational Street Pollution Model (OSPM) – a review of performed application and validation studies, and future prospects, Environ. Chem., 7, 485–503, https://doi.org/10.1071/EN10070, 2010.

Keller, M., Hausberger, S., Matzer, C., Wüthrich, P., and Notter, B.: Handbuch für Emissionsfaktoren des Strassenverkehrs (HBEFA) (handbook of emission factors for road traffic). Version 3.3., Tech. Rep., INFRAS AG, Bern, Switzerland, available at: http://www.hbefa.net/e/documents/HBEFA33_Documentation_20170425.pdf, 2017.

Kuenen, J., Denier van der Gon, H., Visschedijk, A., Van der Brugh, H., and Van Gijlswijk, R.: MACC European emission inventory for the years 2003–2007, TNO-report TNO-060-UT-2011-00588, Utrecht, available at: https://gmes-atmosphere.eu/documents/deliverables/d-emis/TNO_report_UT-00588_MACC_emission2003_2007.pdf, 2011.

Kumar, A., Dixit, S., Varadarajan, C., Vijayan, A., and Masuraha, A.: Evaluation of the AERMOD dispersion model as a function of atmospheric stability for an urban area, Environ. Prog., 25, 141–151, https://doi.org/10.1002/ep.10129, 2006.

Kumar, P., Garmory, A., Ketzel, M., Berkowicz, R., and Britter, R.: Comparative study of measured and modelled number of nanoparticles in an urban street canyon, Atmos. Environ., 43, 949–958, https://doi.org/10.1016/j.atmosenv.2008.10.025, 2009.

Kumar, P., Ketzel, M., Vardoulakis, S., Pirjola, L., and Britter, R.: Dynamics and dispersion modelling of nanoparticles from road traffic in the urban atmospheric environment – a review, J. Aerosol Sci., 42, 580–603, https://doi.org/10.1016/j.jaerosci.2011.06.001, 2011.

Kumar, P., Feiz, A.-A., Ngae, P., Singh, S. K., and Issartel, J.-P.: CFD simulation of short-range plume dispersion from a point release in an urban like environment, Atmos. Environ., 122, 645–656, https://doi.org/10.1016/j.atmosenv.2015.10.027, 2015a.

Kumar, P., Morawska, L., Martani, C., Biskos, G., Neophytou, M., Di Sabatino, S., Bell, M., Norford, L., and Britter, R.: The rise of low-cost sensing for managing air pollution in cities, Environ. Int., 75, 199–205, https://doi.org/10.1016/j.envint.2014.11.019, 2015b.

Lefebvre, W., Vercauteren, J., Schrooten, L., Janssen, S., Degraeuwe, B., Maenhaut, W., de Vlieger, I., Vankerkom, J., Cosemans, G., Mensink, C., Veldeman, N., Deutsch, F., Van Looy, S., Peelaerts, W., and Lefebre, F.: Validation of the MIMOSA-AURORA-IFDM model chain for policy support: modeling concentrations of elemental carbon in Flanders, Atmos. Environ., 45, 6705–6713, https://doi.org/10.1016/j.atmosenv.2011.08.033, 2011.

Lelieveld, J., Barlas, C., Giannadaki, D., and Pozzer, A.: Model calculated global, regional and megacity premature mortality due to air pollution, Atmos. Chem. Phys., 13, 7023–7037, https://doi.org/10.5194/acp-13-7023-2013, 2013.

Li, X.-X., Liu, C.-H., Leung, D. Y. C., and Lam, K. M.: Recent progress in CFD modelling of wind field and pollutant transport in street canyons, Atmos. Environ., 40, 5640–5658, https://doi.org/10.1016/j.atmosenv.2006.04.055, 2006.

Liu, F., Beirle, S., Zhang, Q., Dörner, S., He, K., and Wagner, T.: NO$_x$ lifetimes and emissions of cities and power plants in polluted background estimated by satellite observations, Atmos. Chem. Phys., 16, 5283–5298, https://doi.org/10.5194/acp-16-5283-2016, 2016.

Miranda, A., Silveira, C., Ferreira, J., Monteiro, A., Lopes, D., Relvas, H., Borrego, C., and Roebeling, P.: Current air quality plans in Europe designed to support air quality management policies, Atmos. Pollut. Res., 6, 434–443, https://doi.org/10.5094/APR.2015.048, 2015.

Mueller, M. D., Wagner, M., Barmpadimos, I., and Hueglin, C.: Two-week NO$_2$ maps for the City of Zurich, Switzerland, derived by statistical modelling utilizing data from a routine passive diffusion sampler network, Atmos. Environ., 106, 1–10, https://doi.org/10.1016/j.atmosenv.2015.01.049, 2015.

Mueller, M. D., Hasenfratz, D., Saukh, O., Fierz, M., and Hueglin, C.: Statistical modelling of particle number concentration in Zurich at high spatio-temporal resolution utilizing data from a mobile sensor network, Atmos. Environ., 126, 171–181, https://doi.org/10.1016/j.atmosenv.2015.11.033, 2016.

Oettl, D.: High resolution maps of nitrogen dioxide for the Province of Styria, Austria, Int. J. Environ. Pollut., 54, 137, https://doi.org/10.1504/IJEP.2014.065114, 2014.

Oettl, D.: A multiscale modelling methodology applicable for regulatory purposes taking into account effects of complex terrain and buildings on pollutant dispersion: a case study for an inner Alpine basin, Environ. Sci. Pollut. R., 22, 17860–17875, https://doi.org/10.1007/s11356-015-4966-9, 2015a.

Oettl, D.: Quality assurance of the prognostic, microscale windfield model GRAL 14.8 using wind-tunnel data provided by the German VDI guideline 3783-9, J. Wind Eng. Ind. Aerod., 142, 104–110, https://doi.org/10.1016/j.jweia.2015.03.014, 2015b.

Oettl, D.: Documentation of the GRAMM mesoscale model Vs. 16.1, Tech. Rep., Amt der Steiermaerkischen Lan-

desregierung, Rep. LU-05-16, Graz, Austria, available at: http://app.luis.steiermark.at/berichte/Download/Fachberichte/Lu_05_16_GRAMM_Documentation.pdf, 2016.

Oettl, D. and Hausberger, S.: Simulation of traffic induced NOx-concentrations near the A12 highway in Austria, Atmos. Environ., 40, 6043–6052, https://doi.org/10.1016/j.atmosenv.2005.12.034, 2006.

Oettl, D. and Uhrner, U.: Development and evaluation of GRAL-C dispersion model, a hybrid Eulerian–Lagrangian approach capturing NO–NO_2–O_3 chemistry, Atmos. Environ., 45, 839–847, https://doi.org/10.1016/j.atmosenv.2010.11.028, 2011.

Oettl, D., Sturm, P. J., Bacher, M., Pretterhofer, G., and Almbauer, R. A.: A simple model for the dispersion of pollutants from a road tunnel portal, Atmos. Environ., 36, 2943–2953, https://doi.org/10.1016/S1352-2310(02)00254-6, 2002.

Ottosen, T.-B., Kakosimos, K. E., Johansson, C., Hertel, O., Brandt, J., Skov, H., Berkowicz, R., Ellermann, T., Jensen, S. S., and Ketzel, M.: Analysis of the impact of inhomogeneous emissions in the Operational Street Pollution Model (OSPM), Geosci. Model Dev., 8, 3231–3245, https://doi.org/10.5194/gmd-8-3231-2015, 2015.

Parra, M. A., Santiago, J. L., Martín, F., Martilli, A., and Santamaría, J. M.: A methodology to urban air quality assessment during large time periods of winter using computational fluid dynamic models, Atmos. Environ., 44, 2089–2097, https://doi.org/10.1016/j.atmosenv.2010.03.009, 2010.

Pernigotti, D., Gerboles, M., Belis, C. A., and Thunis, P.: Model quality objectives based on measurement uncertainty. Part II: NO_2 and PM10, Atmos. Environ., 79, 869–878, https://doi.org/10.1016/j.atmosenv.2013.07.045, 2013.

Raaschou-Nielsen, O., Andersen, Z. J., Beelen, R., Samoli, E., Stafoggia, M., Weinmayr, G., Hoffmann, B., Fischer, P., Nieuwenhuijsen, M. J., Brunekreef, B., Xun, W. W., Katsouyanni, K., Dimakopoulou, K., Sommar, J., Forsberg, B., Modig, L., Oudin, A., Oftedal, B., Schwarze, P. E., Nafstad, P., De Faire, U., Pedersen, N. L., Östenson, C.-G., Fratiglioni, L., Penell, J., Korek, M., Pershagen, G., Eriksen, K. T., Sørensen, M., Tjønneland, A., Ellermann, T., Eeftens, M., Peeters, P. H., Meliefste, K., Wang, M., Bueno-de Mesquita, B., Key, T. J., de Hoogh, K., Concin, H., Nagel, G., Vilier, A., Grioni, S., Krogh, V., Tsai, M.-Y., Ricceri, F., Sacerdote, C., Galassi, C., Migliore, E., Ranzi, A., Cesaroni, G., Badaloni, C., Forastiere, F., Tamayo, I., Amiano, P., Dorronsoro, M., Trichopoulou, A., Bamia, C., Vineis, P., and Hoek, G.: Air pollution and lung cancer incidence in 17 European cohorts: prospective analyses from the European Study of Cohorts for Air Pollution Effects (ESCAPE), Lancet Oncol., 14, 813–822, https://doi.org/10.1016/S1470-2045(13)70279-1, 2013.

Ren, X., Harder, H., Martinez, M., Lesher, R. L., Oliger, A., Simpas, J. B., Brune, W. H., Schwab, J. J., Demerjian, K. L., He, Y., Zhou, X., and Gao, H.: OH and HO_2 chemistry in the urban atmosphere of New York City, Atmos. Environ., 37, 3639–3651, https://doi.org/10.1016/S1352-2310(03)00459-X, 2003.

Rood, A. S.: Performance evaluation of AERMOD, CALPUFF, and legacy air dispersion models using the Winter Validation Tracer Study dataset, Atmos. Environ., 89, 707–720, https://doi.org/10.1016/j.atmosenv.2014.02.054, 2014.

Soulhac, L., Salizzoni, P., Cierco, F. X., and Perkins, R.: The model SIRANE for atmospheric urban pollutant dispersion; Part I, Presentation of the model, Atmos. Environ., 45, 7379–7395, https://doi.org/10.1016/j.atmosenv.2011.07.008, 2011.

Soulhac, L., Salizzoni, P., Mejean, P., Didier, D., and Rios, I.: The model SIRANE for atmospheric urban pollutant dispersion; Part II, Validation of the model on a real case study, Atmos. Environ., 49, 320–337, https://doi.org/10.1016/j.atmosenv.2011.11.031, 2012.

Steinbacher, M., Zellweger, C., Schwarzenbach, B., Bugmann, S., Buchmann, B., Ordóñez, C., Prevot, A. S. H., and Hueglin, C.: Nitrogen oxide measurements at rural sites in Switzerland: bias of conventional measurement techniques, J. Geophys. Res., 112, D11307, https://doi.org/10.1029/2006JD007971, 2007.

Stocker, J., Hood, C., Carruthers, D., and McHugh, C.: ADMS-Urban: developments in modelling dispersion from the city scale to the local scale, Int. J. Environ. Pollut., 50, 308, https://doi.org/10.1504/IJEP.2012.051202, 2012.

Terrenoire, E., Bessagnet, B., Rouïl, L., Tognet, F., Pirovano, G., Létinois, L., Beauchamp, M., Colette, A., Thunis, P., Amann, M., and Menut, L.: High-resolution air quality simulation over Europe with the chemistry transport model CHIMERE, Geosci. Model Dev., 8, 21–42, https://doi.org/10.5194/gmd-8-21-2015, 2015.

Thunis, P., Pederzoli, A., and Pernigotti, D.: Performance criteria to evaluate air quality modeling applications, Atmos. Environ., 59, 476–482, https://doi.org/10.1016/j.atmosenv.2012.05.043, 2012.

US Environment Protection Agency: Meteorological monitoring guidance for regulatory modeling applications, Tech. Rep. EPA-454/R-99-005, US Environmental Protection Agency, Office of Air and Radiation, Office of Air Quality Planning and Standards, Research Triangle Park, N.C., 2000.

Van Roosbroeck, S., Wichmann, J., Janssen, N. A. H., Hoek, G., van Wijnen, J. H., Lebret, E., and Brunekreef, B.: Long-term personal exposure to traffic-related air pollution among school children, a validation study, Sci. Total Environ., 368, 565–573, https://doi.org/10.1016/j.scitotenv.2006.03.034, 2006.

Vardoulakis, S., Gonzalez-Flesca, N., and Fisher, B. E. A.: Assessment of traffic-related air pollution in two street canyons in Paris: implications for exposure studies, Atmos. Environ., 36, 1025–1039, https://doi.org/10.1016/S1352-2310(01)00288-6, 2002.